Journal of Alloys and Compounds 778 (2019) 866–877

Contents lists available at ScienceDirect

Journal of Alloys and Compounds

journal homepage: http://www.elsevier.com/locate/jalcom

CO_2 capture by coal ash-derived zeolites- roles of the intrinsic basicity and hydrophilic character

Ana-Paola Beltrao-Nunes [a, b], Radia Sennour [a], Vasilica-Alisa Arus [c], Sarah Anoma [a], Marçal Pires [b], Nabil Bouazizi [d], René Roy [a], Abdelkrim Azzouz [a, *]

[a] Nanoqam, Department of Chemistry, University of Quebec at Montreal, P.O. Box 8888, Succ. Centre-ville, QC, H3C3P8, Canada
[b] Laboratório de Química Analítica Ambiental, Faculdade de Química, Pontifícia Universidade Católica do Rio Grande do Sul, Brazil
[c] Catalysis and Microporous Materials Laboratory, Vasile-Alecsandri University of Bacau, Romania
[d] Ecole Nationale Supérieure des Arts et Industries Textiles, GEMTEX Laboratory, 59056, Roubaix, France

ARTICLE INFO

Article history:
Received 3 July 2018
Received in revised form
30 October 2018
Accepted 10 November 2018
Available online 13 November 2018

Keywords:
Surface basicity
Hydrophilic character
Coal fly ash-derived zeolites
NaP1
Carbon dioxide capture
Greenhouse gases

ABSTRACT

The affinity towards carbon dioxide (CO_2) of coal fly ash-derived zeolites such as 4A, NaP1, zeolite X nanosized and their commercial counterparts was investigated. For this purpose, their surface basicity and hydrophilic character were assessed through thermal programmed desorption measurements (TPD) of CO_2 and water retention capacities (CRC and WRC, respectively). X-ray powder diffraction (XRD) and fluorescence (XRF), scanning electron microscopy (SEM), thermal gravimetric analysis (TGA) and measurements on nitrogen adsorption-desorption isotherms demonstrated the key-roles of the zeolite structure and chemical composition. Decreasing CRC induces a WRC increase, indicating a direct proportionality between the zeolite basicity and hydrophobic character, which are essential requirements for potential applications in the capture of acidic gases. TPD patterns deconvolution revealed an enhancement of the hydrophilic character and weak to medium basicity with increasing Si content at the expense of strong basic sites. All zeolites display at least three strengths in retaining CO_2 and moisture, whose distribution is governed by the structure and chemical composition. Within specific Si/Al range, the partial negative charge of lattice oxygens was found to strongly influence the zeolite basicity and hydrophobic character. These findings are of great interest, because they allow tailoring the surface properties for optimum and reversible capture of greenhouse gases, acidic gasses and volatile organic compounds.

1. Introduction

Greenhouse gas (GHG) emissions, volatile organic compounds (VOC) and solids waste release are major environmental issues that mostly originate from fossil fuels. The latter still remain the main source of energy, and coal consumption generates significant amounts of coal fly ash (CFA) as the main by-product. CFA is one of the most abundant anthropogenic waste materials and causes negative environmental issues when irregularly disposed [1]. Less than 30% of the amount of total production of CFA is reused, more particularly in cement industry. Most CFAs are mixtures of metal oxides such as SiO_2, Al_2O_3, Fe_2O_3, CaO, MgO, K_2O with trace of many other elements [2–5]. Brazilian coal is considered as a low quality residue with low carbon amount and its combustion generate CFA that contains mostly elements such as Si (57,8%), Al (29,06%), Fe (4,8%), K (2,72%), CaO (1,44%) and Ti (1,4%) and residual sulfur (SO_3) [6].

Reuse of industrial wastes such as fly ash, clays and others may be an interesting avenue to explore [4,7]. So far, many reuse attempts have involved CFAs as such in diverse applications or in the preparation of added-value products. There exists an ample literature in this regard, including some examples of CaO- and MgO-enriched CFAs [8,9] and silicalite materials [10] as basic adsorbents, more particularly for the capture of post-combustion CO_2 [11,12]. CFAs can be of great interest when reused or converted into effective adsorbents with sufficient basicity and hydrophilic character for the reversible capture of acidic gases such as CO_2, NOx and SOx and volatile organic compounds (VOC) such as methane.

* Corresponding author.
E-mail address: azzouz.a@uqam.ca (A. Azzouz).

https://doi.org/10.1016/j.jallcom.2018.11.133
0925-8388/

An interesting alternative resides in converting CFAs into zeolites [13,14]. This is possible because CFAs have similar composition as volcanic ash precursors for natural aluminosilicates such as clays, which already turned out to be low cost CO_2 adsorbents [15–18]. However, notwithstanding that zeolites display higher porosity and specific surface area as compared to clay materials, their large scale use is usually limited by production cost constraints [19]. That is why a growing interest is now devoted to CFA-derived zeolites, more particularly when intended for uses in sustainable applications [4,20–23] or to attenuate the impacts of greenhouse gases and VOCs. Most-CFA-derived zeolites showed similar and even higher performances as commercial adsorbents in environmental pollutants removal from both aqueous and gaseous media [13,14,24–27], more particularly in the capture of CO_2, methane and others by physical adsorption [28–33].

The zeolite synthesis selectivity turned out to vary widely from 40 to 75% according to the SiO_2/Al_2O_3 mole ratio of the starting CFA material, and is often affected by the presence of stable contaminants such as hematite (α-Fe_2O_3) and magnetite (Fe_3O_4), α-quartz (SiO_2) and/or mullite ($2SiO_2 \cdot Al_2O_3$). High purity zeolites can only be obtained through energy-consuming procedures [34,35].

Zeolites are known to behave as acidic and hydrophilic materials. Their adsorption capacity of weakly interacting molecules usually increases with the charge density of the exchangeable cations [36–41]. CO_2 molecules are expected to display electrophilic character and both Lewis and Brønsted acidities. Lattice oxygen atoms, more particularly those surrounding exchangeable Si-O-Al groups, act as Lewis bases being an electron pair donor. The partial negative charge of lattice oxygen atoms (PNCLO) is expected to be proportional to the zeolite basicity and Al content [39,42]. In other words, the intrinsic basicity increases with decreasing Si/Al ratio. PNCLO calculations only take into account the zeolite chemical composition [38,43,44] but not the framework structure and surface topology around Si-O-Al groups. These two factors determine specific PNCLO distribution and consequently specific basicity strength on a zeolite surface [39,43]. Besides, the silanol groups are supposed not only to contribute to basicity through their oxygen atoms, but to the hydrophobic character as well. The density of Al atoms induces surface negative charges that influence more or less this hydrophobic character depending to the Si/Al ratio.

All these properties can be judiciously tailored through suitable pre-synthesis procedures according to the applications targeted. According to the Si/Al ratio, a zeolite surface is expected to display specific basicity in capturing specific acidic molecules such CO_2 and specific hydrophobic character in retaining organic molecules like methane and other VOCs. That is why the present work was undertaken. Increased basicity should be beneficial for enhanced interaction with CO_2 [37–41]. However, only optimum basicity strength and hydrophilic character can allow achieving a truly reversible capture of CO_2. This is the main objective of the present research, given that no approach has been tackled so far regarding the role of both surface properties.

The present work was undertaken to demonstrate that adequate zeolites with judiciously tailored basicity and hydrophobic character can be synthesized from CFA, and that these surface properties strongly correlate to the Si/Al ratio. For this purpose, thermal programmed desorption of CO_2 and water (TPD) was employed to determine these two features expressed in terms of CO_2 and water retention capacity (CRC and WRC, respectively) and their strength distributions. Given the special interest devoted to the reversible capture of CO_2 and VOCs, the CRC and WRC will be assessed within a temperature (20–400 °C) that minimizes zeolite denaturation through irreversible dehydroxylation.

2. Experimental

2.1. Zeolites synthesis and modification

CFA-derived zeolites of types 4A, X, Y and NaP1 were synthetized using coal fly ash generated in coal combustion in Thermal Power Plant President Médici (UTPM) in Candiota City, Rio Grande do Sul, Brazil, as previously reported [6]. Analysis of the chemical composition of 99% dry samples of coal fly ash revealed an SiO_2/Al_2O_3 weight ratio of 1.99, with minor amounts of Fe_2O_3 (4.80%), K_2O (2.72), CaO (1.44), TiO_2 (1.40), SO_3 (1.06) and others. In order to investigate the role the Al/Si ratio on the surface basicity and hydrophilic character, different zeolites (Table 1**)** were synthesized via a two steps procedure under moderate operating conditions. Thus, 30.0 g of coal ash was added to 300 mL of 2 M NaOH (99.5%), and the mixture was heated in a water bath at 100 °C for 2 h under continuous stirring. After filtration under vacuum, the filtrate was used for the synthesis of zeolites 4A and X, while the solid residue with depleted Si and Al content was employed for NaP1 zeolite synthesis. Both steps were performed by conventional hydrothermal process in a closed PTFE reactor, yielding high purity zeolites (82–95%, 4A and X) and medium grade zeolite (61% NaP1), respectively.

Zeolite X with nanosized crystals was synthesized from pure compounds based on literature methodologies [45–47]. A gel synthesis with high alkalinity and aging step resulted in a decrease in the final particle size. Sodium aluminate and sodium hydroxide was dissolved into deionized water to form a transparent solution, then silica source was added and the resulting mixture was stirred at room temperature to obtain a homogeneous hydrogel. This gel was transferred to Teflon-lined stainless-steel autoclaves, then aged for 3 days at room temperature and further hydrothermally treated at 100 °C at 6 h. The final product was washed and filtrated until pH 9, then dried at 60 °C for 2 h, and further calcined for 1 h at 400 °C and stored in sealed glass enclosure. Some zeolites such as NaP1 and nanozeolite X were washed with deionized water until pH 7 in order to remove possible residues of soluble reagents and/or impurities.

2.2. Characterization

All samples, including the starting CFA, were characterized through X-Ray diffraction (XRD) (Siemens D5000 instrument, Co-K_{alpha} at 1.7890 Å), X-ray fluorescence (XRF) (Brücker AXS S4 Pioneer instrument) and thermal gravimetric analysis (TGA) (Q5000)/(Discovery MS equipment under a 10.0 mL min^{-1} helium stream and 5 °C.min^{-1} heating rate). The particle morphology and chemical composition were analyzed by scanning electron microscopy (SEM, model XL 30 Philips with coupled to an Energy Dispersion X-ray fluorescence AX system). The thermal stability was assessed between 20 °C and 800 °C. The particle size distribution of powder zeolites was determined by laser diffraction particle size analysis (Master-sizer 3000, Malvern Instruments Ltd, using wet dispersion on water). FTIR spectra were recorded using a Perkin Elmer Spectrum 100 FTIR spectrophotometer. Textural characterization (surface area and porosity) was performed using N_2 adsorption-desorption isotherms and a Micrometrics Tristar II 3020 instrument after samples outgassing at 120 °C under vacuum for 12 h. The specific surface area (SSA) was calculated by the Brunauer, Emmett and Teller (BET) method. The pore size distribution was assessed by Barrett, Joyner and Halenda (BJH) model.

2.3. Measurements by thermal programmed desorption (TPD)

Thermal programmed desorption measurements were achieved

Table 1
Si/Al mole ratio of the zeolites synthesized.

Samples	Si/Al (mol.mol^{-1})	Origin/Synthesis procedure
Coal Fly Ash	2.39	Originating from coal combustion in a thermal Power, Brazil
NanoX	1.58	Zeolite nanosized from pure reagents
NanoX washed	1.57	Synthesized from pure reagents washed repeatedly with distillated water
X	1.09	Zeolites synthetized from coal fly ashes
13 X	1.24	Commercial product provided by Industrias Químicas del Ebro (IQE), Spain, washed as a part of the commercial synthesis
NaP1	1.09	Zeolites synthetized from coal fly ashes
NaP1washed	1.09	Zeolites synthetized from coal fly ash washed repeatedly with distillated water
NaP1commercial		Commercial product provided by Industrias Químicas del Ebro (IQE), Spain, washed as a part of the commercial synthesis
4A	0.93	Commercial product provided by IQE, Spain, washed as a part of the commercial synthesis
4A washed	1.03	Synthesized from coal fly ashes washed repeatedly with distillated water

using N60 pure grade carbon dioxide (CO_2) and nitrogen (N_2) [48–50]. A 45–50 mg amount of each sample with 0.1–0.2 mm particle size was introduced in the cylindrical glass microreactor (2 mm internal diameter) of the oven coupled to a detector Li-840A dual CO_2/H_2O Gas Analyser (Li-COR Bioscience Inc., USA). The zeolite samples were previously calcined at 400 °C for 1 h under a dry air flow (15 mL min^{-1}), at normal pressure in order to remove adsorbed gases and possible traces or carbonates before TPD measurements and rehydrated to free air at ambient conditions. For specific TPD analysis of CO_2 adsorption without the effect of moisture, the samples were dehydrated at 140 °C at 5 °C.min^{-1} heating rate during 40 min before saturation. For qualitative assessment of the basicity strength distribution, saturation was carried out by progressive injection of an excess of dry CO_2 (10–30 mL) through the samples (45–50 mg) for 20–30 min under a 15 mL min^{-1} nitrogen stream at ambient conditions. For accurate calculation of CO_2 retention capacity, the samples were contacted with ca. 100 mL dry CO_2 for 24 h under a 5 mL min^{-1} nitrogen stream or in a static mode without nitrogen stream. The excess CO_2 was purged at room temperature under dry N_2 flow until the CO_2 concentration was approximately 10 ppm. A first TPD run (TPD1) was performed at 5 °C.min^{-1} heating rate from 20 °C to 450 °C under a 5 mL min^{-1} nitrogen stream. This was repeated twice (TPD2 and TPD3) without rehydration, but after re-saturation with dry CO_2 under similar conditions. The hydrophilic character was assessed through H_2O-TPD measurements according the same procedure. The basicity and hydrophilic character were expressed in terms of CO_2 and water retention capacities (CRC and WRC respectively), and were defined as the area described by their corresponding TPD patterns within the temperature range given by TGA measurements. For avoiding zeolite denaturation through irreversible dehydroxylation, the basicity and hydrophobic character were assessed between 20 °C and 450 °C. The retention strength distribution was evaluated by TPD pattern deconvolution (OriginLab® student software, version 2016).

3. Results and discussion

3.1. Structure and stability of unmodified zeolites

Samples X and 4A showed only characteristic XRD reflections (Fig. 1). This is a precise indicator of a high purity, as well argued by the fact that no change in the XRD pattern was noticed after repeated washings. In contrast, NaP1 displayed an additional and common peak with CFA, presumably due to impurities such as quartz or/and mullite. X-ray diffraction revealed high crystallinity for all CFA-derived zeolites, as supported by sharp XRD lines similar to those of commercial counterparts. This is well supported by SEM images that show typical morphology such as, for instance, that of faced cubes for zeolite 4A. Similar observation can be made for the other zeolite samples, which also displayed well-defined crystalline particles (Fig. 2).

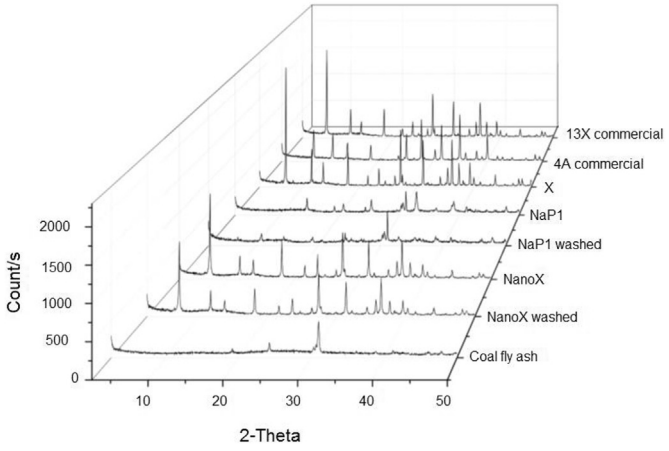

Fig. 1. XRD patterns of coal fly ash and derived zeolites as compared to commercial counterparts.

TGA measurements showed almost similar TGA patterns, characterized by a predominant and common endothermal process starting from ca.70–80 °C due to dehydration for all samples (Fig. 3). Weight loss assessment provided a first evaluation of the hydrophilic character of the non-dehydrated zeolites samples.

As expected, different zeolites showed various weight losses. The lowest water content (7.5% and 8.5%, resp.) were registered for NaP1 and, to a lesser extent, its washed counterpart. This can be explained, at least partly, by the lowest specific surface area (SSA = 38 m^2 g^{-1}), pore size (0.2 nm) and porosity (0.2 cm^3 g^{-1}) (Table 2). The relatively wide range of dehydration temperature which extends up to 500 °C for NaP1 washed is a specific feature of low-porosity zeolites, and suggests the occurrence slow water vapor removal due to diffusion hindrance within the internal porosity. The low water losses of NaP1 and its washed counterpart agree with their lowest water retention capacity (CRC) of 9.38 and 1.72 μmol g^{-1}, respectively, and can also be explained by higher content in hydrophobic impurities such as amorphous phases, quartz and mullite (ca. 61%) as compared to the other zeolites (5–18%).

As expected the highest dehydration grade of up to 20 wt% were noticed for highly porous zeolite such as Nano-X, X, 14X and, to a lesser extent, both 4A samples. Unlike the latter and 4A, the other samples showed a clear plateau starting from 250 °C up to 575 °C.

This indicates the end of the dehydration process and appreciable thermal stability of these zeolites, as was supported by fairly similar TPD patterns obtained after successive TPD-rehydration cycles between 20 °C and 200 °C. Nevertheless, it is worth emphasizing that the hydrophilic character cannot be assessed only

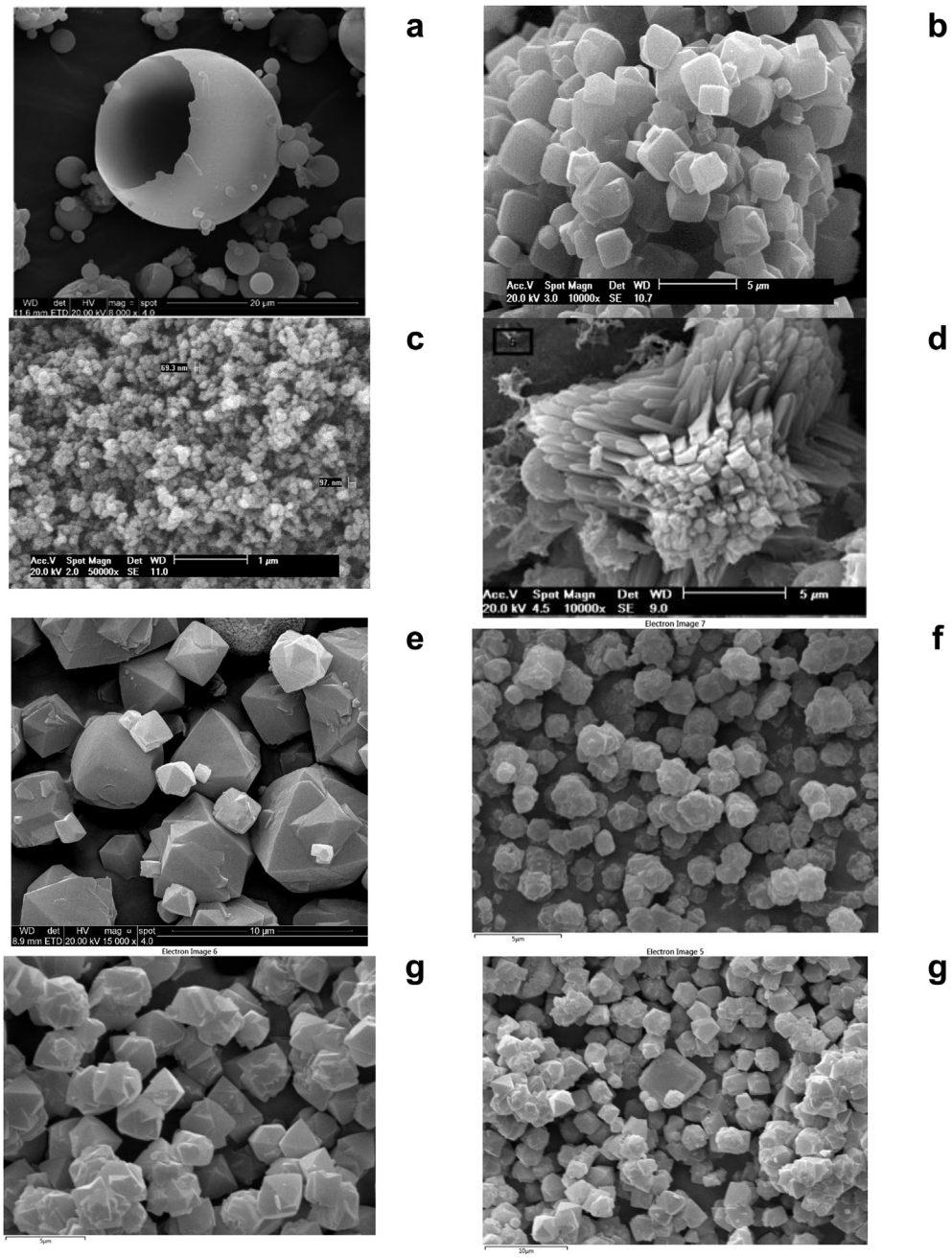

Fig. 2. SEM images of CFA (a) and derived zeolites: b. 4A; c. NanoX; d. NaP1; e. X (from fly ash); f. Y (IQE); g,h. 13X.

on the basis of TG measurements. Other factors such as the chemical composition expressed in terms of Si/Al ratio must also have a certain contribution. Indeed, FTIR analysis showed higher intensity of the broad bands at 3500–3000 cm^{-1} for high silica zeolite such as faujasite Y (Si/Al = 2.40 mol mol^{-1}) as compared to 13X (Si/Al = 1.24) NaP1 (Si/Al = 1.09) and 4A (Si/Al = 1.0) (Fig. 4).

This Si/Al decrease sequence is similar to that of the intensity of the 1230–1060 cm^{-1} and 800-790 cm^{-1} bands corresponding to the asymmetric and symmetric stretching vibration of Si–O–Si bridge, but with that of the 1630-1620 cm^{-1} assigned to the adsorbed water on the surface. This observation suggests the influence other parameters, presumably the framework structure, the in-plane/out-of plane silanol ratio and thereby the acid-base properties of the surface. This will be examined further through thermal programmed desorption of carbon dioxide.

3.2. *Affinity towards CO_2*

CO_2 adsorption on zeolites should also involve acid-base interaction, and the amount of both Brønsted must play key roles in the retention and strength retention of CO_2 and water [51]. CO_2 is a conventional probe molecule for investigating the basicity of metal oxides and zeolites. Preliminary experiments through overnight saturation of the most efficient zeolite for CO_2 capture, namely NaP1 showed a marked intensity increase of the 3600-3000 cm^{-1} band (Fig. 5). This allows predicting a key role of the surface hydroxyl groups in the affinity towards CO_2. The slight intensification of the 800-900 cm^{-1} and 1650 cm^{-1} bands suggests additional

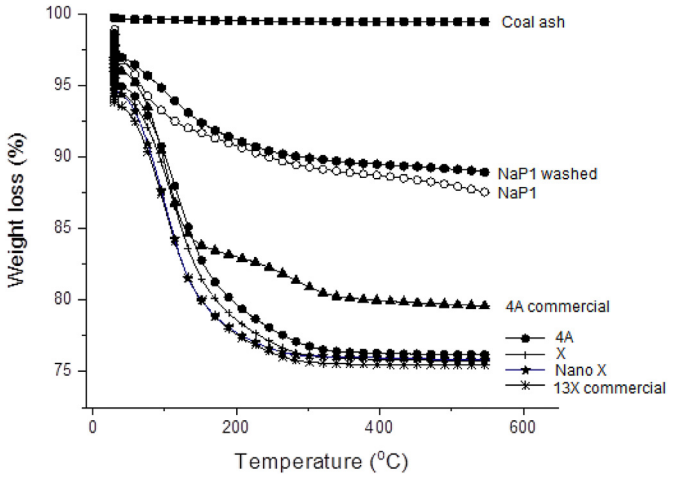

Fig. 3. TGA patterns of coal ash and derived zeolites.

contributions the Si–O–Si bridges, presumably through the electron pair of the lattice oxygen and of the absorbed water, respectively.

Deeper insights in the zeolite affinity for CO_2 were achieved through temperature-programmed desorption (TPD), which is an appropriate method that provides valuable information in this regard [52]. As expected, the different zeolites displayed TPD patterns that differ both in shape and amount of desorbed CO_2 (Fig. 6). This provides evidence of the role of the chemical and framework structure. The persistence of CO_2 and water desorption at a constant temperature of 400 °C for 20 min (a step-wise TPD run) (Fig. 5) accounts for appreciable thermal stability of all zeolites in agreement with previous TGA analysis.

The presence of various desorption peaks indicates the occurrence of a distribution of different CO_2 retention strengths and, subsequently, a basicity strength distribution. As a common feature, repeated TPD runs without periodical rehydration (TPD2 and TPD3) induced changes in the shape of CO_2-TPD patterns (Figs. S1–S5, Fig. 7).

Similar observation can be made for H_2O-TPD patterns that reflect the hydrophilic character (Fig. S6). Fairly similar CO_2-TPD patterns but completely flat H_2O-TPD pattern were obtained after TPD4 and TPD5, indicating total dehydration of the zeolite samples. This result suggests that water plays a certain role in CO_2 retention, and provides clear evidence that calcination up to 400 °C did not produce irreversible processes, and that dehydroxylation, if any, should be entirely reversible.

3.3. CO_2 and water retention capacities

Repeated TPD attempts without rehydration resulted in a decay in the basicity expressed in terms of CRC decrease (Fig. 8). The fact that TPD1 (in black) gave higher CRC as compared to TPD2 and TPD3 must be due to water contribution to CO_2 adsorption in agreement with previous data [16,18,53–56]. TPD1 should

Table 2
CO_2 and H_2O retention capacities of all CFA-derived zeolites.

Samples	Particle size D_{50} (μm)	Si/Al mol.mol^{-1}	S_{BET} (m^2.g^{-1})	Pore		Mass loss %**	WRC (μmol.g^{-1})	CRC (μmol.g^{-1})
				Size (nm)	Volume (cm^3.g^{-1})			
Coal ash	24	2.39	–	–	–	0.44 (20–400 °C)	0.0	237.3
Faujasite Y	4.7 ± 0.1	2.40	747	3.3	3.3	–	84.88	78.1
Nano X	0.08	1.58	653	0.1	0.1	7.5 (80–120 °C)	32.14	318.2
Nano Xwashed	–	1.57	–	–	–	22.24 (20–400 °C)	34.29	144.9
13X	10.1 ± 0.6	1.24	670	2.8	2,8	21% (100 °C) 2.0% (3.25 °C)	29.20	117.5
NaP1	2.3 ± 0.1	1.09	38	0.2	0.2	11.6 (20–400 °C)	9.38	399.2
NaP1 washed	–	1.09	–	–	–	9.84 (80–120 °C)	1.72	206.1
X	15.3 ± 0.7	1.09	423	2.0	2.0	21.7 (20–400 °C)	17.22	285.7
4A washed	–	1.03	–	–	–	22.05 (20–400 °C)	24.79	200.3
4A	4.8 ± 0.5	1.0	405	0.2	0.2	7.27 (152 °C) 2.6% (375 °C)	14.99	170.4

* The CO_2 and H_2O Retention Capacities (CRC and WRC, respectively) were assessed from average TPD pattern area calculated from the three TPD runs. ** As determined by TG analysis. The approximate temperature of the correction endo peak, as determined by DTG analysis, is provided between brackets.

Table 3
CO_2 retention capacity of NaP1 as compared with other materials.

Sample	CRC (μmol.g^{-1})	Surface area (m^2.g^{-1})	Temperature range (°C)	Ref.
Na-montmorillonite (NaMt)	685	49–52	20–100	[54]
CuMt	53	–	20–100	[54]
CaMt	97	37–38	20–100	[54]
Acid-activated bentonite	250–260	86–138	20–450	[57]
MgAl – Layered Double Hydroxide (MgAl-LDH)	1500–2500	–	20–240	[58]
SBA-15 silica	132–317	577	20–400	[59]
Fe/SBA-15	148–454	572	20–400	[59]
SBA-15	14.5–52.0	800	20–80	[50]
SBA-16	9.3–19.5	–	20–80	[50]
Na-MCM-41 zeolite	13–26	–	20–80	[50]
Na-Omega zeolite	486	118.4	20–600	[60]
Amine-loaded zeolites	360	–	–	[61]
Multiwalled carbon nanotubes (MW-CNT)	980	–	–	[62]
Co-loaded cocoa-shell derived hydrochar	1350	<30	–	[63]
NaP1	399	38	20–100	This work

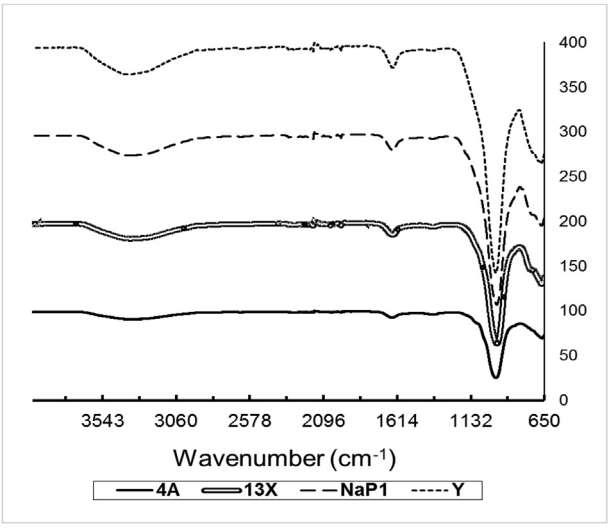

Fig. 4. FTIR spectra of some CFA-derived zeolites.

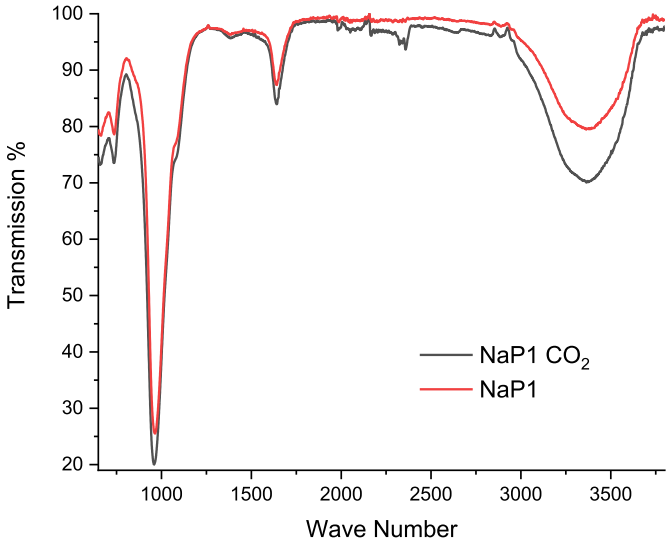

Fig. 5. FTIR spectra of NaP1 before and after overnight saturation with dry CO_2.

correspond to the maximum CRC including water contribution, while TPD3 is supposed to provide the lowest CRC value that reflects the intrinsic surface basicity.

This effect of dehydration appears to be specific to each zeolite, presumably due to specific distributions of the adsorption sites. Repeated TPD runs without rehydration was also found to induce changes in the strength distribution of the basicity, more particularly regarding the weakest basicity sites. Here, water removal from the solid surface is supposed to unveil the intrinsic acidity of the zeolite surface, which mostly consists of Lewis acidity in the absence of moisture [64]. NaP1 displayed the highest CRC value (399 μmol g^{-1}) (Table 2). The latter is obviously lower than that reported for well-known basic MgAl-LDHs, carbon nanotubes and hydrochar-based adsorbents but, interestingly, almost in the same magnitude order as for amine-loaded zeolites (360 μmol g^{-1}) and even higher that for more acidic mesoporous silicas and ion-exchanged and acid-activated clays minerals (Table 3).

3.4. Effect of zeolite washing

The washing process with distilled water also induced changes in the CRC value and distribution of the basicity strength (Fig. S7). For instance, 4A washing produced increases in CRC from 170.4 to 200.4 μmol g^{-1} and in WRC from 14.99 to 24.79 μmol g^{-1}, due to an elimination of soluble and acidic impurities such as calcium and iron sulphates (Table S1). This was accompanied by an increase in the amounts of medium and strong basic sites (from 8.12 to 19.50% and from 40.40 to 75.79%, respectively) at the expense of that of weak basicity, which markedly dropped from 50.49 down to 4.71%. Similar effects of the washing were noticed for zeolite 4A.

An almost reverse behavior was noticed for Nano X with a CRC decay from 318.2 to 144.9 μmol g^{-1}. The marked enhancement of the weak basicity from 4.09 to 47.63% at the expense of medium and strong basic sites (from 55.95 to 34.46% and from 39.96 to 17.36%, respectively) must be due to a removal of base-like impurities, presumably residual CFA. For Na-P1, the decreases in WRC (from 9.38 to 1.72 μmol g^{-1}) and WRC (from 399.2 to 206.1 μmol g^{-1}), respectively must mainly arise from sodium and iron chloride leaching (Table S1). This was accompanied by an improvement of medium basicity (from 1.70 to 9.82%) at the expense of the amount of strong basic sites (from 71.04 to 64.59%), while that of weak basicity remained almost constant.

3.5. Distribution of the basicity strength

The occurrence of multiple desorption peaks suggests a clear heterogeneity of the surface basicity, which is expressed in terms of basicity strength distribution (BSD). Deeper insights in the BSD involved TPD pattern deconvolution, assuming that CO_2 adsorption-desorption equilibrium conditions generate perfectly symmetric desorption peak, and that the basicity strength is proportional to the desorption temperature [48]. The results revealed specific BSD according to the structure of the synthesized zeolite, its Si/Al ratio and surface topology. Numerous deconvoluted TPD patterns were obtained, only those of zeolites X and NaP1 are presented herein (Fig. 9, S8-S10). Na-P1 showed three predominant basicity strengths, which appear to be common features of all zeolites [50], but with specific distribution of CO_2 adsorption sites (COS) for each zeolite. These basic sites should be attributed not only to the lattice oxygens surrounding the −Si-O-Al Brønsted acid sites [38,43,50,65] but also to terminal and weakly basic silanols similar to those of mesoporous silicas [65].

The intrinsic basicity of the lattice oxygen atoms (O-atoms) strongly depends on the location of the Si-O-Al exchangeable sites. Around a central Al atom, the strong basicity is assumed to be induced by the O-atoms belonging to the second tetrahedral layer (Scheme 1). Medium and weak basicity are rather assigned to more peripheral layers [39].

Na^+ cations are expected to display very weak Lewis acidity due to their large size and small charge (Low polarizing capacity). Various Si/Al ratios induce different amount of Na^+ cation on the zeolite surface. Therefore, different interactions are expected to occur with different zeolites frameworks at different locations within a given framework [66]. The distribution strength is expected to narrowly correlate to the number of next-neighboring tetrahedra around a given exchangeable site, and, thereby strongly depends on the lattice structure and topology [65,67]. This explains the variability of the basicity strength distribution according to the zeolite type. Besides, the silanol groups should exert their basicity through the electron pair of the oxygen atom of the OH bond.

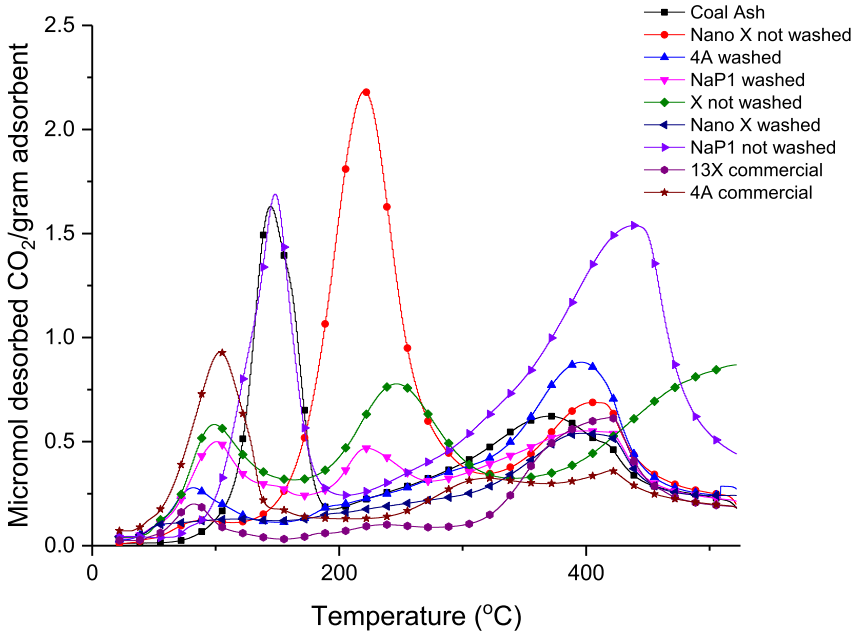

Fig. 6. First CO_2 TPD patterns for all zeolites (TPD1) at 5 °C.min^{-1} heating rate, after saturation with dry CO_2 for 20–30 min in a static mode and a purge of the excess CO_2 at room temperature under dry N_2 flow.

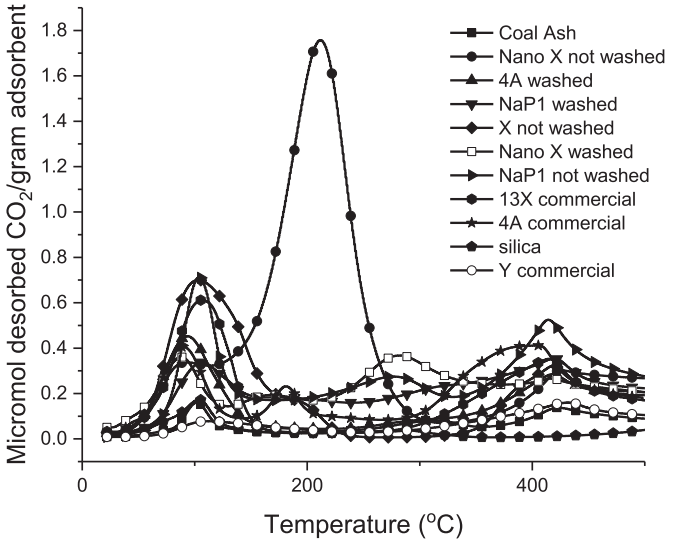

Fig. 7. Average CO_2-TPD patterns for all zeolites. These patterns were obtained from average measurements obtained from TPD2 and TPD3. The latter were performed after TPD1 without rehydration, but after saturation with dry CO_2 for 20–30 min in a static mode and a purge of the excess CO_2 at room temperature under dry N_2 flow. The desorption peak appearing at 400 °C is due to the fact that temperature was maintained constant at this value for 20 min, and corresponds to a step-wise TPD run of this strong basicity.

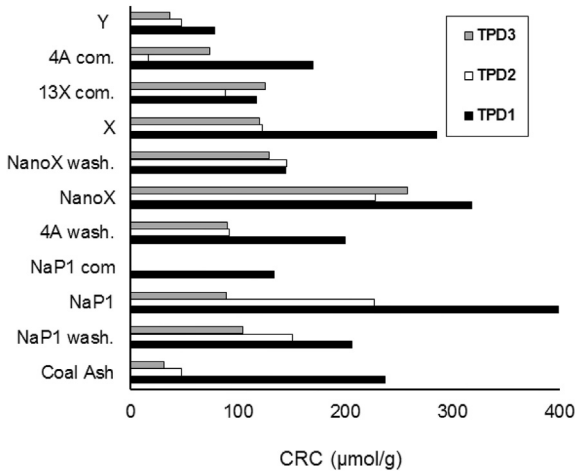

Fig. 8. CO_2 retention capacity of CFA-derived zeolites. TPD1 was performed on fresh sample. TPD2 and TPD3 are two consecutive TPD attempts performed without rehydration and after saturation and purge under the same operating conditions.

Regardless to their location inside the zeolite framework, all lattice oxygens are supposed to act as electron pair donor according the same pathway, while CO_2 molecules should behave as Lewis acid. This is supposed to give rise to carbonate-like associations similar to that occurring with water molecules (Scheme 2). The latter have already been reported in other works [16,53,68–71], and can be more or less stable according to the strength of the Lewis basicity of the oxygen atoms, and, subsequently to its location and surface topology.

In the absence of water molecules, such C:O-lattice bridges can be easily decomposed upon slight heating or even at room temperature under vacuum or forced convection with carrier gas, and must account for weak to medium basic sites that promote purely physical adsorption of CO_2. Chemical CO_2 adsorption, if any, should involve stronger basicity mainly attributed to interaction with water molecules. This was supported by the reversible intensity attenuation of the desorption peaks at high temperature (300-350 °C) after successive TPD runs without periodical rehydration.

Moderate increase of temperature is known to induce change in the distribution strength, but severe heating may also trigger a progressive conversion of Brønsted acid sites into Lewis ones. For most zeolites, this dehydroxylation process was found to be reversible as long as heating did not exceed 400 °C, as supported by TGA analysis and repeated TPD-rehydration cycles within this temperature range.

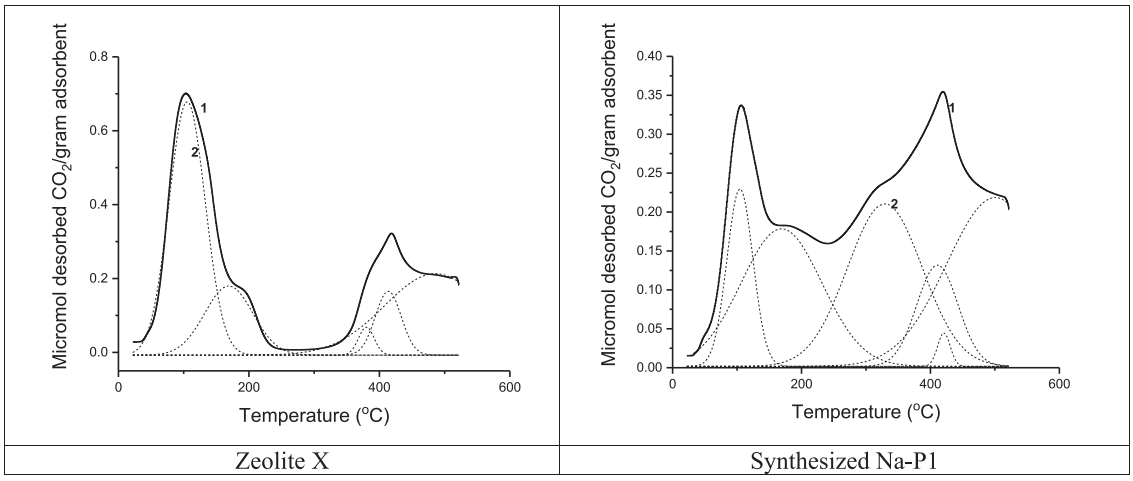

Fig. 9. Peak deconvolution through Gaussian model for CO_2-TPD media pattern. Na-P1 was repeatedly washed with distilled water at room temperature. (1) Experimental curve resulting from TPD measurements; (2) calculated curves obtained using Origin deconvolution software. The 400 °C desorption peak arises by maintaining temperature constant at this value for 20 min, and corresponds to a step-wise TPD measurement of this strong basicity.

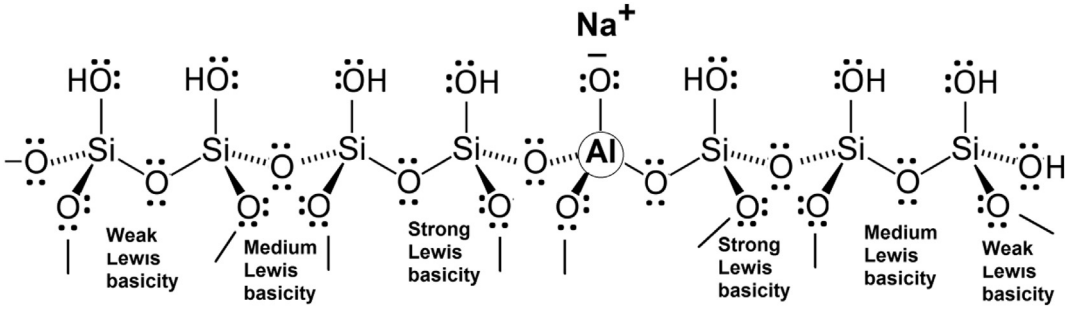

Scheme 1. Basicity strength distribution around an –Si-O-Al-O-Si- exchangeable site.

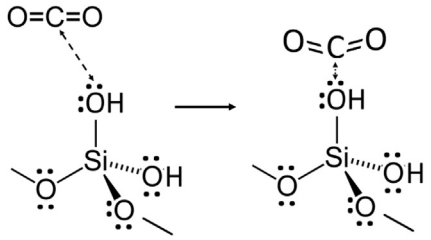

Scheme 2. Genesis of carbonate-like association via CO_2 - lattice oxygen interaction.

3.6. *Effect of Si/Al ratio*

Clear dependence of both the SSA and partial negative charge of lattice oxygens (PNCLO) on the Si/Al ratio was noticed (Fig. 10). The general tendency is that increasing Si/Al ratio improves the SSA but reduces the PNCLO absolute value. The dispersion of the experimental data arises mainly from PNCLO calculations, which include the presence of residual impurities in the chemical composition of the zeolite. For instance, the highest CRC of NaP1 (399.2 μmol g^{-1}) contrasts with its lowest SSA (38 m^2 g^{-1}) (Table 2). This explains the weak correlation between the CRC and Si/Al ratio, in spite of the slight CRC decay for high Si content (Fig. S11).

Conversely, highly pure faujasite Y displayed the highest SSA (747 m^2 g^{-1}) for lowest CRC (78.1 μmol g^{-1}) (Table 2), which agrees with its well-known higher acidity reflected by its higher Si/Al ratio (2.54) and lowest PNCLO (−0.248) as compared to NaP1 (1.0950 and −0.2698, respectively). In zeolite frameworks, high Si content implies more cross-connected channels and edge structure, and, hence, higher acidity, due to higher number of acidic out-of-plane silanols (pKa 5.6 versus pKa 8.5 for in-plane silanols) [72].

As previously stated, PNCLO calculations [44,73,74] are not reliable without taking into account additional effects due to the chemical composition, channel/cavity configuration and arrangements and textural properties. The fact that zeolites with low to moderate specific surface area of 200–500 m^2 g^{-1}, i.e. with low Si content gave high PNCLO values (−0.27: 0.28) (Fig. 11-a). This accounts for high Lewis basicity.

Deeper insights in the role of Si content revealed that increasing Si/Al ratio promotes weak to medium basicity at the expense of strong basic sites (Fig. 11-b). This must be due to low density of Si-O-Al exchangeable sites known to be surrounded by lattice O-atoms with relatively strong Lewis basicity [39] and increased amount of moderately to weakly basic silanols.

This surprisingly high CRC of NaP1 must be due exclusively to multilayer condensation of CO_2 around basic sites via physical interaction involving carbonate-like association [16,53,54,70,75]. This phenomenon is expected to be enhanced by high Al content and subsequently by high number of exchangeable alkali metal cations [38,74,76]. The latter such as Na^+ in NaP1 are known to behave as weak Lewis acids due to their large size and small charge.

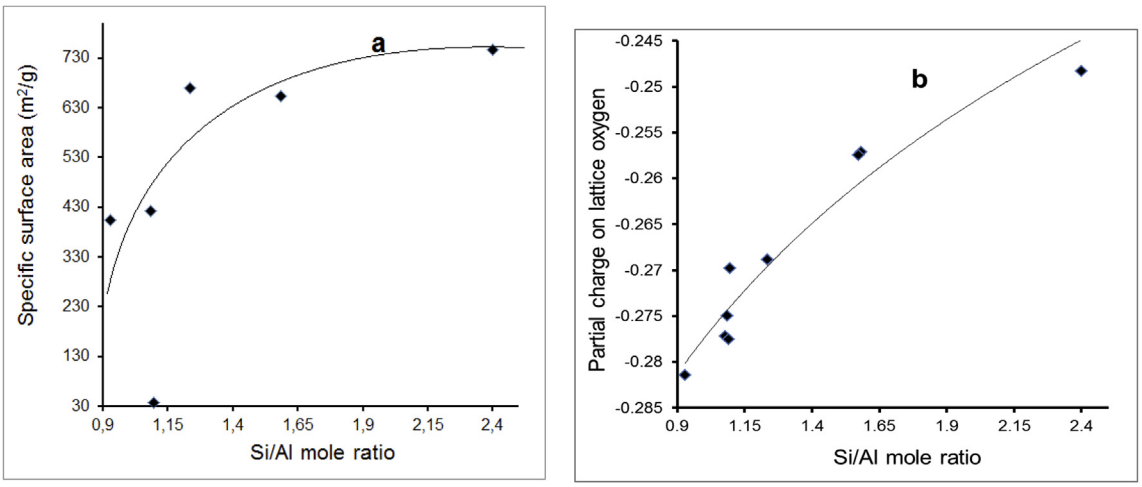

Fig. 10. Specific surface area (a) and partial negative charge on lattice oxygen (b) versus Si/Al mole ratio.

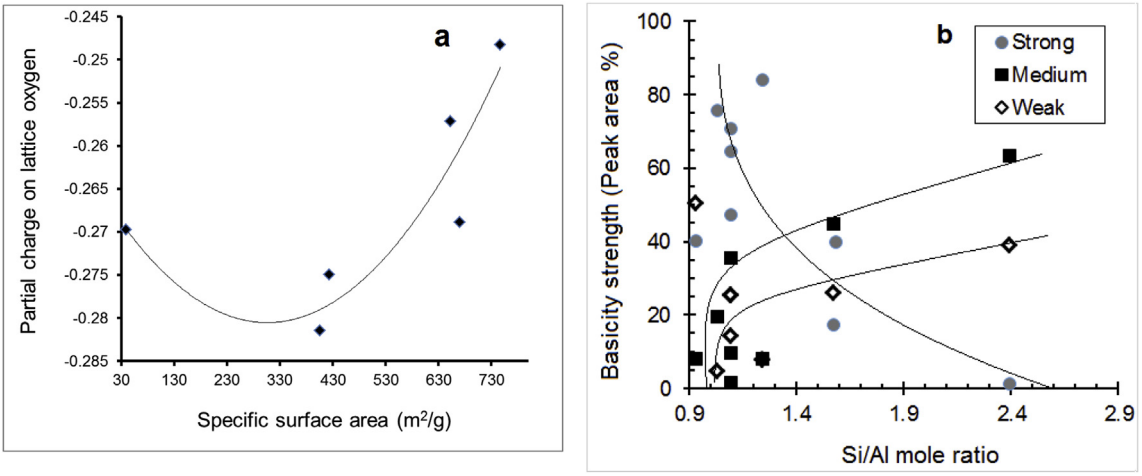

Fig. 11. Partial charge on lattice oxygen versus specific surface area (a) and basicity strength distribution versus Si/Al ratio (b).

Na^+ cations should be concentrated inside the zeolite cavities, resulting in heterogeneously distributed basicity that promotes effective but non-stoichiometric CO_2 condensation around these cavities.

3.7. Hydrophilic character

Most H_2O-TPD patterns started with dehydration at temperature of 60–80 °C according to the zeolite structure, except for some of them (Fig. 12, S1b, S3, S4b-S5b). The fact that water still desorbs even after 140 °C suggests strong moisture retention and strong hydrophilic character. Interestingly, except for NaP1 (washed or not) and silica, water release still persisted even after 250–300 °C for the other zeolites. This must be due to overlapped desorption processes involving delayed dehydration and early dihydroxylation, when both physically retained and structural water are simultaneously released.

There exists an almost linear proportionality between the WRC and Si/Al mole ratio (Fig. 13). This result contrasts with the well-known hydrophobic character of high silica materials. The most plausible explanation resides in the fact that high Si-zeolite are characterized by a predominance of polar edge structures displaying higher acidity and affinity towards water. This result is in agreement with the slight CRC decrease with increasing Si/Al ratio (Fig. S11) and reverse proportionality between the CRC and WRC (Fig. 14).

In other words, the most hydrophobic zeolites should exhibit the highest affinity for carbon dioxide. The hydrophilic character was already found to vary according to the [out-of-plane/in-plane silanol] ratio of mesoporous silicas [65,67,72,77]. Consequently, the silanol groups should also contribute to the affinity towards water or VOCs provided that they exhibit low basicity. This still remains to be elucidated, and investigations are still in progress in this direction.

4. Conclusion

The results obtained herein allow concluding that coal ash-

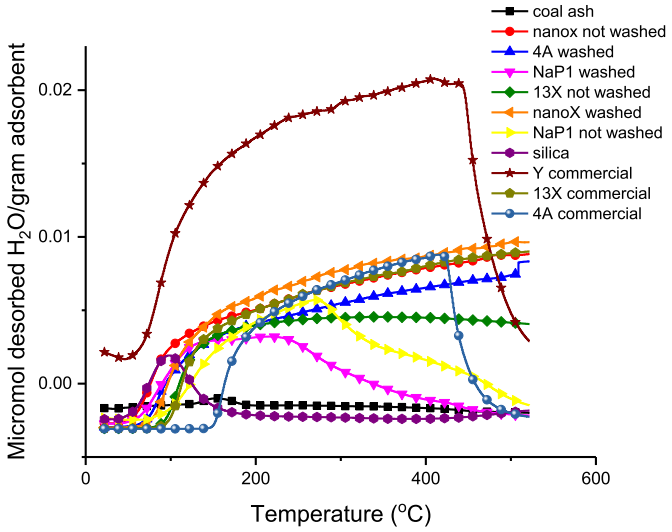

Fig. 12. H_2O-TPD patterns for calcined and rehydrated zeolites samples, These patterns were obtained after saturation with dry CO_2 for 20–30 min in a static mode and a purge of the excess CO_2 room temperature under dry N_2 flow, The desorption peak appearing at 400 °C is due to the fact that temperature was maintained constant at this value for 20 min, and corresponds to a step-wise TPD measurement of this strong basicity.

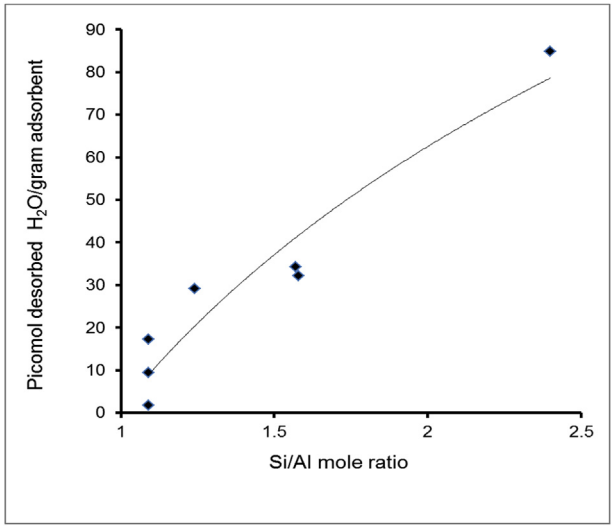

Fig. 13. Water retention capacity (WRC) versus Si/Al mole ratio, These values arise from H_2O-TPD patterns of different zeolite samples obtained after saturation with dry CO_2 for 20–30 min in a static mode and a purge of the excess CO_2 room temperature under dry N_2 flow.

derived zeolites exhibit sufficient base properties and hydrophilic character. Zeolites Na-P1 unwashed, nanoX and zeolite X showed highest affinity towards CO_2. Decreasing CRC induces a WRC increase, indicating a direct proportionality between the zeolite basicity and hydrophobic character, which are essential requirements for potential applications in the capture of acidic gasses and volatile organic compounds (VOC) such as methane. All zeolites display at least three strengths in retaining CO_2 and moisture, whose distribution is governed by the structure and chemical composition. Higher Si/Al ratios were found to improve weak to medium basicity at the expense of strong basic sites, and, paradoxically, to improve the hydrophilic character. The washing process appears to be unnecessary when targeting CO_2 and VOC capture purposes. These

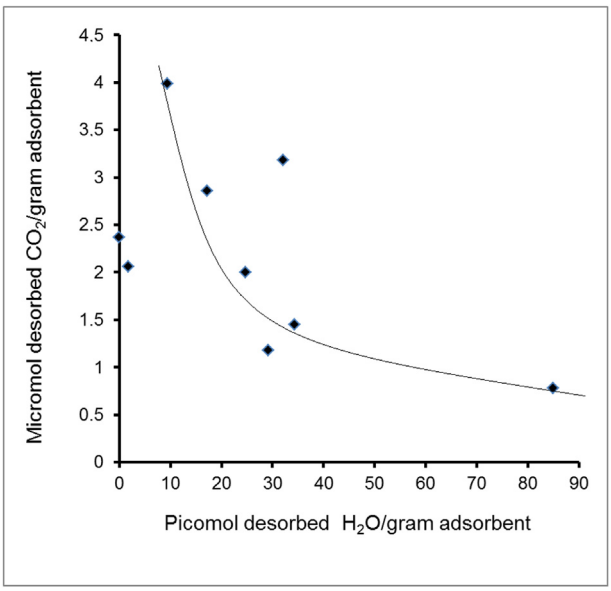

Fig. 14. CO_2 retention capacity (WRC) versus Water retention capacity (WRC), These values arise from CO_2 and H_2O-TPD patterns of different zeolite samples obtained after saturation with dry CO_2 for 20–30 min in a static mode and a purge of the excess CO_2 room temperature under dry N_2 flow.

findings are of great interest, because they allow envisaging the synthesis of zeolites with judiciously tailored properties for the reversible capture of greenhouse gas.

Acknowledgements

The authors' thanks go to CNPq (Bazil) for support to zeolite synthesis project and to CAPES (Brazil) for funding A.P.Beltrao-Nunes. The experimental study of this work was achieved in Pr. A. Azzouz's laboratory at UQAM, Montréal, Canada, and was supported by a grant from MDEIE-FQRNT to R.R and A.A.

Appendix A. Supplementary data

Supplementary data to this article can be found online at https://doi.org/10.1016/j.jallcom.2018.11.133.

References

[1] Z.T. Yao, X.S. Ji, P.K. Sarker, J.H. Tang, L.Q. Ge, M.S. Xia, Y.Q. Xi, A comprehensive review on the applications of coal fly ash, Earth Sci. Rev. 141 (2015) 105–121.
[2] O. Lucon, J. Goldemberg, Sao Paulo–the "other" Brazil: different pathways on climate change for state and federal governments, J. Environ. Dev. 19 (2010) 335–357.
[3] C.Ö. Karacan, F.A. Ruiz, M. Cotè, S. Phipps, Coal mine methane: a review of capture and utilization practices with benefits to mining safety and to greenhouse gas reduction, Int. J. Coal Geol. 86 (2011) 121–156.
[4] W.H. Chan, M.N. Mazlee, Z.A. Ahmad, M.A.M. Ishak, J.B. Shamsul, The development of low cost adsorbents from clay and waste materials: a review, J. Mater. Cycles Waste Manag. 19 (2017) 1–14.
[5] J.d.C. Izidoro, D.A. Fungaro, F.S. dos Santos, S. Wang, Characteristics of Brazilian coal fly ashes and their synthesized zeolites, Fuel Process. Technol. 97 (2012) 38–44.
[6] V.L.V. Fallavena, C.S.d. Abreu, T.D. Inácio, M. Pires, C.M.N. Azevedo, I.D. Fernandes, L.S. Ferret, M.R. Martinez Tarazona, Caracterização detalhada de material de referência certificado de carvão brasileiro, Quím. Nova 36 (2013) 859–864.
[7] L.S. de Carvalho, E. Silva, J.C. Andrade, J.A. Silva, M. Urbina, P.F. Nascimento, F. Carvalho, J.A. Ruiz, Low-cost mesoporous adsorbents amines-impregnated for CO2 capture, Adsorption 21 (2015) 597–609.
[8] B. Sreenivasulu, I. Sreedhar, B.M. Reddy, K.V. Raghavan, Stability and carbon capture enhancement by coal-fly-ash-doped sorbents at a high temperature, Energy Fuels 31 (2017) 785–794.

[9] A. Kaithwas, M. Prasad, A. Kulshreshtha, S. Verma, Industrial wastes derived solid adsorbents for CO_2 capture: a mini review, Chem. Eng. Res. Des. 90 (2012) 1632–1641.
[10] Y. Yan, Y. Gao, W. Tang, Q. Li, J. Zhang, Characterization of high-alumina coal fly ash based silicate material and its adsorption performance to CO_2, Kor. J. Chem. Eng. 33 (2016) 1369–1379.
[11] A. Samanta, A. Zhao, G.K.H. Shimizu, P. Sarkar, R. Gupta, Post-combustion CO_2 capture using solid sorbents: a review, Ind. Eng. Chem. Res. 51 (2012) 1438–1463.
[12] C. Siriruang, P. Toochinda, P. Julnipitawong, S. Tangtermsirikul, CO_2 capture using fly ash from coal fired power plant and applications of CO_2-captured fly ash as a mineral admixture for concrete, J. Environ. Manag. 170 (2016) 70–78.
[13] A.M. Cardoso, M.B. Horn, L.S. Ferret, C.M.N. Azevedo, M. Pires, Integrated synthesis of zeolites 4A and Na–P1 using coal fly ash for application in the formulation of detergents and swine wastewater treatment, J. Hazard. Mater. 287 (2015) 69–77.
[14] A.M. Cardoso, A. Paprocki, L.S. Ferret, C.M.N. Azevedo, M. Pires, Synthesis of zeolite Na-P1 under mild conditions using Brazilian coal fly ash and its application in wastewater treatment, Fuel 139 (2015) 59–67.
[15] A.V. Ursu, G. Jinescu, F. Gros, I.D. Nistor, N.D. Miron, G. Lisa, M. Silion, G. Djelveh, A. Azzouz, Thermal and chemical stability of Romanian bentonite, J. Therm. Anal. Calorim. 106 (2011) 965–971.
[16] A. Azzouz, S. Nousir, N. Platon, K. Ghomari, G. Hersant, J.-Y. Bergeron, T.C. Shiao, R. Rej, R. Roy, Preparation and characterization of hydrophilic organo-montmorillonites through incorporation of non-ionic polyglycerol dendrimers derived from soybean oil, Mater. Res. Bull. 48 (2013) 3466–3473.
[17] A. Azzouz, S. Nousir, N. Bouazizi, R. Roy, Metal-inorganic-organic matrices as efficient sorbents for hydrogen storage, ChemSusChem 8 (2015) 800–803.
[18] S. Nousir, A.-S. Sergentu, T.C. Shiao, R. Roy, A. A, Hybrid clay nanomaterials with improved affinity for carbon dioxide through chemical grafting of amino groups, Int. J. Environ. Pollut Remed. 2 (2014) 58–65.
[19] J.A. Boscoboinik, S. Shaikhutdinov, Exploring zeolite chemistry with the tools of surface science: challenges, opportunities, and limitations, Catal. Lett. 144 (2014) 1987–1995.
[20] S. Wang, H. Wu, Environmental-benign utilisation of fly ash as low-cost adsorbents, J. Hazard. Mater. 136 (2006) 482–501.
[21] G.G. Hollman, G. Steenbruggen, M. Janssen-Jurkovičová, A two-step process for the synthesis of zeolites from coal fly ash, Fuel 78 (1999) 1225–1230.
[22] X. Querol, N. Moreno, J.C. Umaña, A. Alastuey, E. Hernández, A. López-Soler, F. Plana, Synthesis of zeolites from coal fly ash: an overview, Int. J. Coal Geol. 50 (2002) 413–423.
[23] H. Tanaka, Y. Sakai, R. Hino, Formation of Na-A and -X zeolites from waste solutions in conversion of coal fly ash to zeolites, Mater. Res. Bull. 37 (2002) 1873–1884.
[24] K.-M. Lee, Y.-M. Jo, Synthesis of zeolite from waste fly ash for adsorption of CO_2, J. Mater. Cycles Waste Manag. 12 (2010) 212–219.
[25] L. Liu, R. Singh, P. Xiao, P.A. Webley, Y. Zhai, Zeolite synthesis from waste fly ash and its application in CO_2 capture from flue gas streams, Adsorption 17 (2011) 795–800.
[26] J.d.C. Izidoro, D.A. Fungaro, J.E. Abbott, S. Wang, Synthesis of zeolites X and A from fly ashes for cadmium and zinc removal from aqueous solutions in single and binary ion systems, Fuel 103 (2013) 827–834.
[27] C.-H. Lee, S.-W. Park, S.-S. Kim, Breakthrough analysis of carbon dioxide adsorption on zeolite synthesized from fly ash, Kor. J. Chem. Eng. 31 (2014) 179–187.
[28] A. Alonso, J. Moral-Vico, A. Abo Markeb, M. Busquets-Fite, D. Komilis, V. Puntes, A. Sanchez, X. Font, Critical review of existing nanomaterial adsorbents to capture carbon dioxide and methane, Sci. Total Environ. 595 (2017) 51–62.
[29] S.-Y. Lee, S.-J. Park, A review on solid adsorbents for carbon dioxide capture, J. Ind. Eng. Chem. 23 (2015) 1–11.
[30] B. Sreenivasulu, I. Sreedhar, P. Suresh, K.V. Raghavan, Development trends in porous adsorbents for carbon capture, Environ. Sci. Technol. 49 (2015) 12641–12661.
[31] R. Ben-Mansour, M.A. Habib, O.E. Bamidele, M. Basha, N.A.A. Qasem, A. Peedikakkal, T. Laoui, M. Ali, Carbon capture by physical adsorption: materials, experimental investigations and numerical modeling and simulations – a review, Appl. Energy 161 (2016) 225–255.
[32] J.M. Huck, L.-C. Lin, A.H. Berger, M.N. Shahrak, R.L. Martin, A.S. Bhown, M. Haranczyk, K. Reuter, B. Smit, Evaluating different classes of porous materials for carbon capture, Energy Environ. Sci. 7 (2014) 4132–4146.
[33] M. Younas, M. Sohail, L.K. Leong, M.J. Bashir, S. Sumathi, Feasibility of CO_2 adsorption by solid adsorbents: a review on low-temperature systems, Int. J. Environ. Sci. Technol. 13 (2016) 1839–1860.
[34] W. Franus, M. Wdowin, M. Franus, Synthesis and characterization of zeolites prepared from industrial fly ash, Environ. Monit. Assess. 186 (2014) 5721–5729.
[35] C.A.F. Rocha Junior, S.C.A. Santos, C.A.G. Souza, R.S. Angélica, R.F. Neves, Síntese de zeólitas a partir de cinza volante de caldeiras: caracterização física, química e mineralógica, Cerâmica 58 (2012) 43–52.
[36] D. Barthomeuf, Acidity and basicity in zeolites, in: G. Öhlmann, H. Pfeifer, R. Fricke (Eds.), Studies in Surface Science and Catalysis, Elsevier, 1991, pp. 157–169.
[37] G. Busca, Acidity and basicity of zeolites: a fundamental approach, Microporous Mesoporous Mater. 254 (2017) 3–16.
[38] R.A. Schoonheydt, P. Geerlings, E.A. Pidko, R.A. van Santen, The framework basicity of zeolites, J. Mater. Chem. 22 (2012) 18705–18717.
[39] D. Barthomeuf, Framework induced basicity in zeolites, Microporous Mesoporous Mater. 66 (2003) 1–14.
[40] M.N. Mikhailov, V.B. Kazansky, L.M. Kustov, Intensities of IR stretching bands as a criterion of the strength of Lewis acid sites in ZSM-5 zeolites with bivalent cations, Catal. Lett. 116 (2007) 81–86.
[41] C. Busco, A. Barbaglia, M. Broyer, V. Bolis, G.M. Foddanu, P. Ugliengo, Characterisation of Lewis and Brønsted acidic sites in H-MFI and H-BEA zeolites: a thermodynamic and ab initio study, Thermochim. Acta 418 (2004) 3–9.
[42] D. Barthomeuf, G. Coudurier, J.C. Vedrine, Basicity and basic catalytic properties of zeolites, Mater. Chem. Phys. 18 (1988) 553–575.
[43] J. Xie, M. Huang, S. Kaliaguine, Zeolite basicity characterized by chloroform chemisorption, An infrared study, Reaction Kinetics and Catalysis Letters 58 (1996) 217–227.
[44] M. Huang, S. Kaliaguine, Zeolite basicity characterized by pyrrole chemisorption: an infrared study, J. Chem. Soc., Faraday Trans. 88 (1992) 751–758.
[45] D. Hu, Q.H. Xia, X.H. Lu, X.B. Luo, Z.M. Liu, Synthesis of ultrafine zeolites by dry-gel conversion without any organic additive, Mater. Res. Bull. 43 (2008) 3553–3561.
[46] T.F. Chaves, H.O. Pastore, D. Cardoso, A simple synthesis procedure to prepare nanosized faujasite crystals, Microporous Mesoporous Mater. 161 (2012) 67–75.
[47] T. Poznyak, R. Tapia, J. Vivero, I. Chairez, J. Mex Chem. Soc. 50 (2006) 28.
[48] A. Azzouz, D. Nistor, D. Miron, A.V. Ursu, T. Sajin, F. Monette, P. Niquette, R. Hausler, Assessment of acid–base strength distribution of ion-exchanged montmorillonites through NH3 and CO_2-TPD measurements, Thermochim. Acta 449 (2006) 27–34.
[49] S. Nousir, N. Platon, K. Ghomari, A.S. Sergentu, T.C. Shiao, G. Hersant, J.Y. Bergeron, R. Roy, A. Azzouz, Correlation between the hydrophilic character and affinity towards carbon dioxide of montmorillonite-supported polyalcohols, J. Colloid Interface Sci. 402 (2013) 215–222.
[50] I. Terrab, B. Boukoussa, R. Hamacha, N. Bouchiba, R. Roy, A. Bengueddach, A. Azzouz, Insights in CO_2 interaction on zeolite omega-supported polyol dendrimers, Thermochim. Acta 624 (2016) 95–101.
[51] F. Lónyi, J. Valyon, On the interpretation of the NH_3-TPD patterns of H-ZSM-5 and H-mordenite, Microporous Mesoporous Mater. 47 (2001) 293–301.
[52] O. Klepel, B. Hunger, Temperature-programmed desorption (TPD) of carbon dioxide on alkali-metal cation-exchanged faujasite type zeolites, J. Therm. Anal. Calorim. 80 (2005) 201–206.
[53] A. Azzouz, N. Platon, S. Nousir, K. Ghomari, D. Nistor, T.C. Shiao, R. Roy, OH-enriched organo-montmorillonites for potential applications in carbon dioxide separation and concentration, Separ. Purif. Technol. 108 (2013) 181–188.
[54] A. Azzouz, A.-V. Ursu, D. Nistor, T. Sajin, E. Assaad, R. Roy, TPD study of the reversible retention of carbon dioxide over montmorillonite intercalated with polyol dendrimers, Thermochim. Acta 496 (2009) 45–49.
[55] S. Nousir, N. Platon, K. Ghomari, A.-S. Sergentu, T.C. Shiao, G. Hersant, J.-Y. Bergeron, R. Roy, A. Azzouz, Correlation between the hydrophilic character and affinity towards carbon dioxide of montmorillonite-supported polyalcohols, J. Colloid Interface Sci. 402 (2013) 215–222.
[56] K.G. S. Nousir, R. Roy, A. Azzouz, Polyol–clay matrices with improved hydrophilic character and affinity towards CO_2 - attempts to CO_2 concentration at room temperature, Nanotech 2013 Chapter 9: carbon Capture, Bio Sensors, Instruments, Medical, Environment and Energy (Volume 3) 701 - 704.
[57] V.A. Arus, S. Nousir, R. Sennour, T.C. Shiao, I.D. Nistor, R. Roy, A. Azzouz, Intrinsic affinity of acid-activated bentonite towards hydrogen and carbon dioxide, Int. J. Hydrogen Energy 43 (2018) 7964–7972.
[58] A. Azzouz, V.-A. Aruş, N. Platon, K. Ghomari, I.-D. Nistor, T.C. Shiao, R. Roy, Polyol-modified layered double hydroxides with attenuated basicity for a truly reversible capture of CO_2, Adsorption 19 (2013) 909–918.
[59] N. Bouazizi, R. Ouargli, S. Nousir, R.B. Slama, A. Azzouz, Properties of SBA-15 modified by iron nanoparticles as potential hydrogen adsorbents and sensors, J. Phys. Chem. Solid. 77 (2015) 172–177.
[60] A. Hakiki, B. Boukoussa, Z. Kibou, I. Terrab, K. Ghomari, N. Choukchou-Braham, R. Hamacha, A. Bengueddach, A. Azzouz, Correlation of hydrophilic character and surface basicity of exchanged omega-catalyzed MCR process, Thermochim. Acta 662 (2018) 108–115.
[61] R. Chatti, A.K. Bansiwal, J.A. Thote, V. Kumar, P. Jadhav, S.K. Lokhande, R.B. Biniwale, N.K. Labhsetwar, S.S. Rayalu, Amine loaded zeolites for carbon dioxide capture: amine loading and adsorption studies, Microporous Mesoporous Mater. 121 (2009) 84–89.
[62] F. Su, C. Lu, W. Cnen, H. Bai, J.F. Hwang, Capture of CO_2 from flue gas via multiwalled carbon nanotubes, Sci. Total Environ. 407 (2009) 3017–3023.
[63] J. Vieillard, N. Bouazizi, R. Bargougui, N. Brun, P. Fotsing Nkuigue, E. Oliviero, O. Thoumire, N. Couvrat, E. Djoufac Woumfo, G. Ladam, N. Mofaddel, A. Azzouz, F. Le Derf, Cocoa shell-derived hydrochar modified through aminosilane grafting and cobalt particle dispersion as potential carbon dioxide adsorbent, Chem. Eng. J. 342 (2018) 420–428.
[64] T. Cseri, S. Békássy, F. Figueras, S. Rizner, Benzylation of aromatics on ion-exchanged clays, J. Mol. Catal. A Chem. 98 (1995) 101–107.
[65] I. Terrab, R. Ouargli, B. Boukoussa, K. Ghomari, R. Hamacha, R. Roy, A. Azzouz, A. Bengueddach, Assessment of the intrinsic interactions of mesoporous silica with carbon dioxide, Res. Chem. Intermed. 43 (7) (2017) 3775–3786.
[66] G. Busca, Chapter 7 - zeolites and other structurally microporous solids as acid–base materials. Heterogeneous Catalytic Materials, Elsevier, Amsterdam,

2014, pp. 197–249.
[67] R. Ouargli, S. Larouk, I. Terrab, R. Hamacha, N. Benharrats, A. Bengheddach, A. Azzouz, Intrinsic activity of SBA-like silica in the catalytic ozonation of organic pollutants, Ozone: Sci. Eng. 38 (2016) 48–61.
[68] Aylmore, Gas sorption in clay mineral systems, Clay Clay Miner. 22 (1974) 175–183.
[69] J.J. Gassensmith, H. Furukawa, R.A. Smaldone, R.S. Forgan, Y.Y. Botros, O.M. Yaghi, J.F. Stoddart, Strong and reversible binding of carbon dioxide in a green metal–organic framework, J. Am. Chem. Soc. 133 (2011) 15312–15315.
[70] A. Azzouz, E. Assaad, A.-V. Ursu, T. Sajin, D. Nistor, R. Roy, Carbon dioxide retention over montmorillonite–dendrimer materials, Appl. Clay Sci. 48 (2010) 133–137.
[71] A. Azzouz, S. Nousir, N. Platon, K. Ghomari, T.C. Shiao, G. Hersant, J.-Y. Bergeron, R. Roy, Truly reversible capture of CO_2 by montmorillonite intercalated with soya oil-derived polyglycerols, Int. J. Greenhouse Gas Contr. 17 (2013) 140–147.
[72] M. Sulpizi, M.-P. Gaigeot, M. Sprik, The silica–water interface: how the silanols determine the surface acidity and modulate the water properties, J. Chem. Theor. Comput. 8 (2012) 1037–1047.
[73] R.T. Sanderson, Chemical Bonds and Bond Energy, Academic Press, 1971.
[74] M. Huang, S. Kaliaguine, A. Auroux, Lewis basic and Lewis acidic sites in zeolites, Stud. Surf. Sci. Catal. 97 (1995) 311–318.
[75] N. Bouazizi, D. Barrimo, S. Nousir, R. Ben Slama, R. Roy, A. Azzouz, Montmorillonite-supported Pd^0, Fe^0, Cu^0 and Ag^0 nanoparticles: properties and affinity towards CO_2, Appl. Surf. Sci. 402 (2017) 314–322.
[76] A.L. Allred, Electronegativity values from thermochemical data, J. Inorg. Nucl. Chem. 17 (1961) 215–221.
[77] S. Larouk, R. Ouargli, D. Shahidi, L. Olhund, T.C. Shiao, N. Chergui, T. Sehili, R. Roy, A. Azzouz, Catalytic ozonation of Orange-G through highly interactive contributions of hematite and SBA-16 - to better understand azo-dye oxidation in nature, Chemosphere 168 (2017) 1648–1657.